The WIYN telescope active optics system

Nicolas Roddier, Dan Blanco, Larry Goble
National Optical Astronomy Observatories[•]
PO Box 26732, Tucson, AZ 85726-6732

Claude Roddier
Institute for Astronomy, University of Hawaii
2680 Woodlawn Dr., Honolulu, HI 96822

ABSTRACT

In this paper we describe the active optics system of the WIYN 3.5 meter telescope which will go into operation in the spring of 1995 on Kitt Peak, Arizona. The active optics system provides real time collimation of the telescope and optical figure control of the primary mirror. The individual subsystems are first described. These include the wavefront curvature sensing technique, the support and articulation of the secondary mirror, the control of the primary mirror figure and rigid body motion, and the mechanics and electronics used for controlling and monitoring the optics. Algorithms for the complete loop are then discussed. This involves mapping coma terms used to actively correct the collimation, while residual phase errors are corrected by active control of the forces supporting the primary mirror. In the next section we compare two operational modes: open loop using mapped collimation and optical figure corrections, and closed loop using feedback from the wavefront sensor directly. Finally, preliminary stellar images obtained with the actively controlled telescope are presented.

1. INTRODUCTION

The WIYN telescope is a joint project of the University of Wisconsin, Indiana University, Yale University, and the National Optical Astronomy Observatories to build a 3.5 meter ground-based telescope on Kitt Peak, Arizona[1,2]. The telescope is now in engineering trials prior to full science operation later this year.

This paper describes the components and use of active optics in the WIYN telescope. The telescope and facility incorporate many strategies aimed at delivering the best images available at the site. The intrinsic quality of the polished optics is excellent[3]; the temperature of the primary mirror is controlled[4]; the dome, telescope and all optics are of lightweight, low thermal inertia construction; the telescope and dome are both actively and passively ventilated[5]. Active optics should be viewed as an important part of an integrated overall design. The WIYN telescope is shown in figure 1.

2. SYSTEM OVERVIEW

The goal of the WIYN active optics system is to maintain the optical quality of the telescope at a consistently high level. This is done in two ways: the telescope is actively collimated by controlling the position of the secondary mirror, and the figure of the primary mirror is controlled[6,7,8] to remove residual aberrations introduced by the entire optical train including the secondary and tertiary mirrors, and any transmissive optics in the beam.

The active optics system consists of the primary mirror and support, the secondary mirror and its support and articulation, the wavefront sensor, the control electronics, and the control algorithms to bring these pieces together as a system. The individual subsystems are described in the next sections. A functional block diagram is shown in figure 2.

[•] Operated by the Association of Universities for Research in Astronomy, Inc. (AURA) under cooperative agreement with the National Science Foundation.

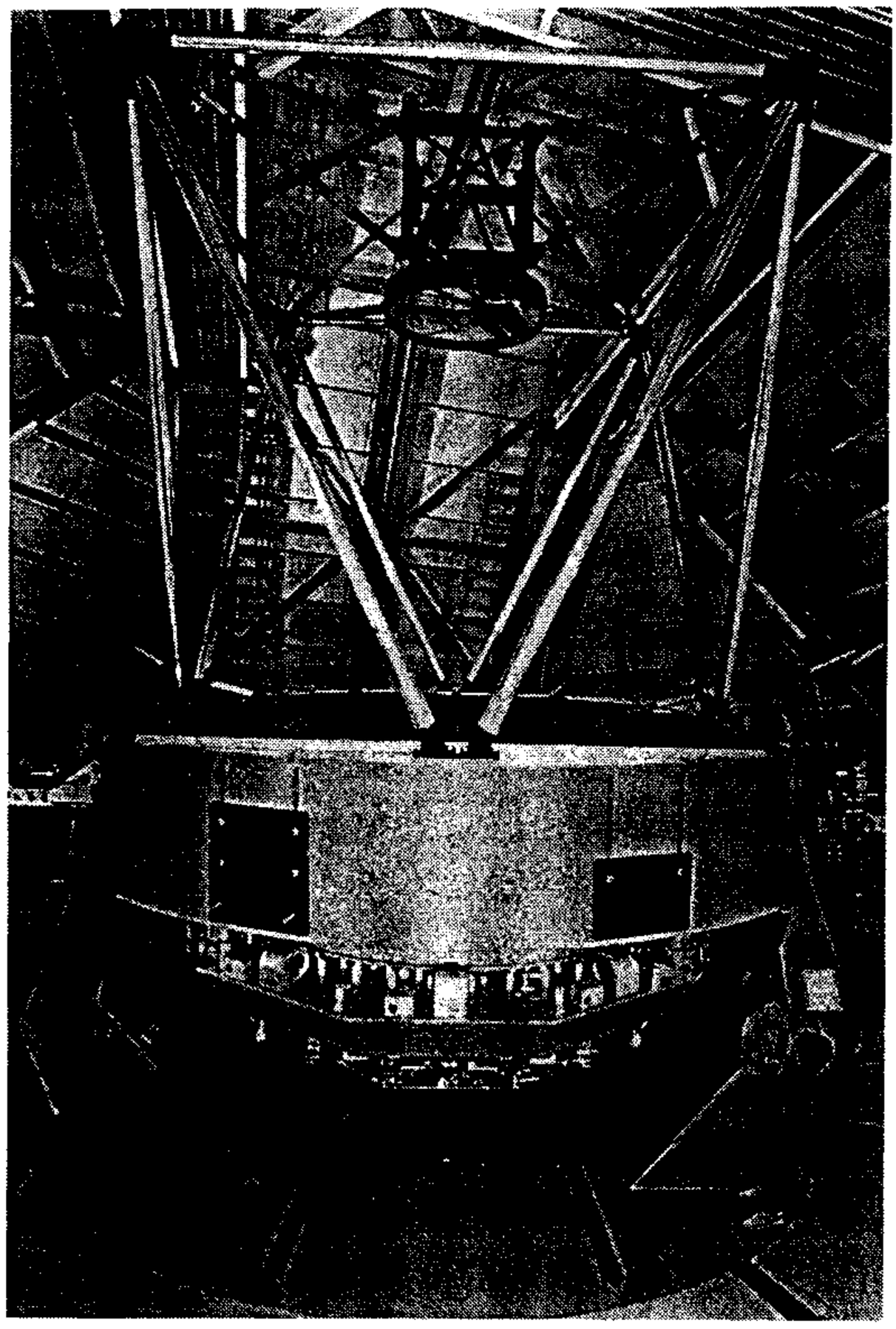

Figure 1. The WIYN Telescope.

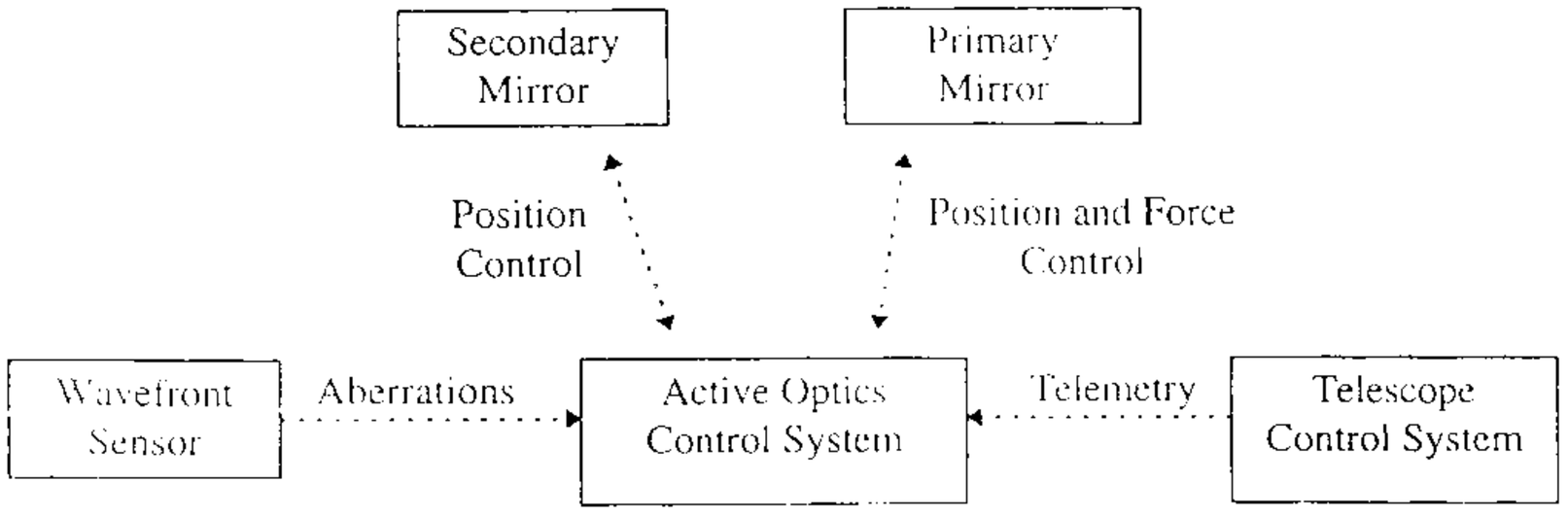

Figure 2. Functional block diagram of the WIYN active optics system.

3. PRIMARY MIRROR AND SUPPORT

The 3.5m primary mirror is a borosilicate glass honeycomb spin casting from the University of Arizona Mirror Lab[9]. It is of low mass and high stiffness to reduce thermal inertia and to limit gravity distortion. However, for active optics we need to bend the glass. The mirror is sensitive to forces applied in the axial direction but relatively insensitive to forces applied in the lateral direction (in the plane of the disk). This led us to separate the lateral from the axial supports. Lateral supports are totally passive while the axial supports combine passive and active support forces.

3.1 Primary passive support

A hydraulic support system to float the mirror was chosen[6,7,8]. This offers a significant advantage because it is inherently stiff against wind forces. Hydraulic supports require some extra complexity to counteract hydrostatic head pressure. The WIYN design turns this complexity to an advantage by making the passive system tuneable.

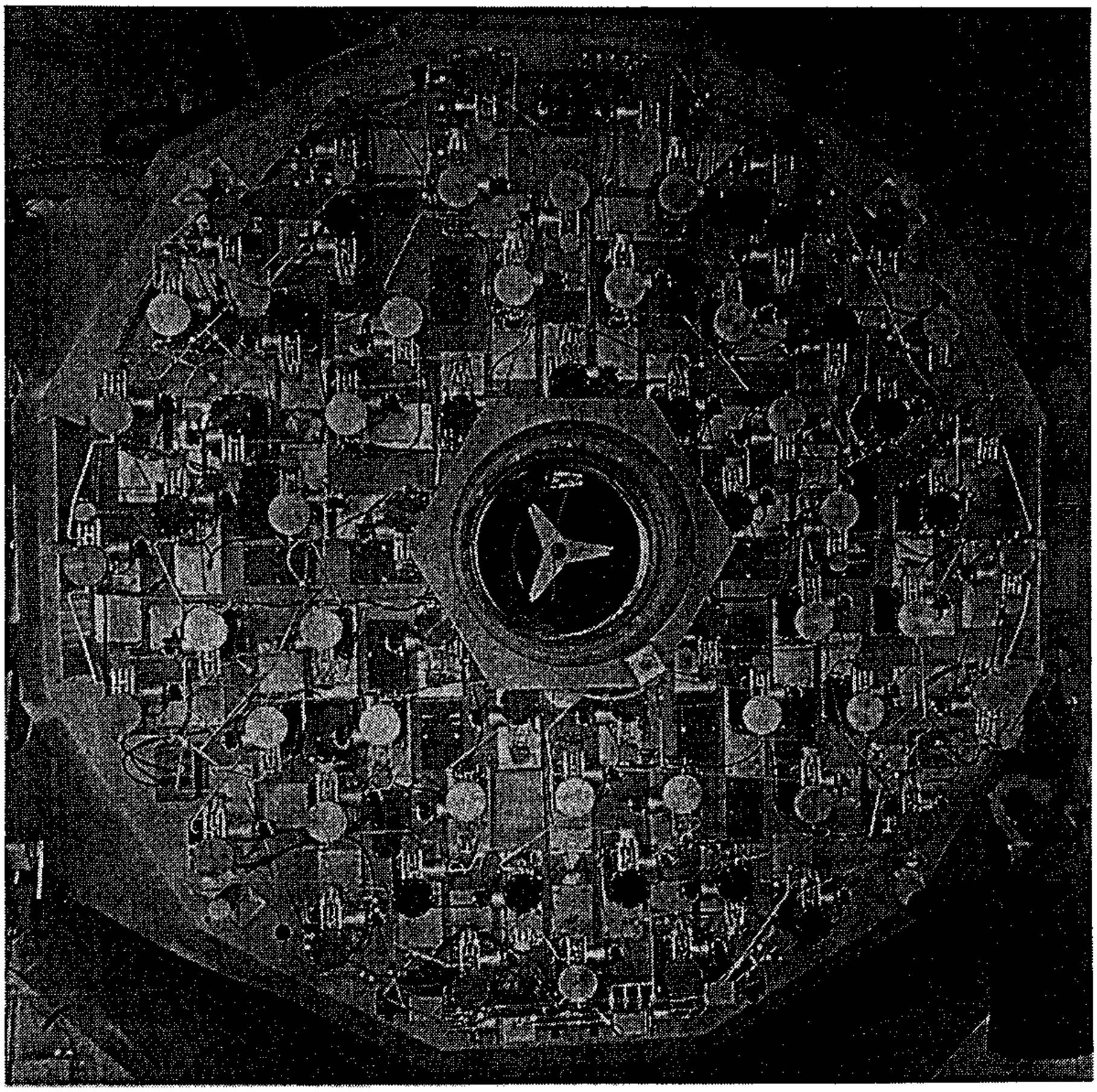

Figure 3. The WIYN mirror cell showing the axial supports.

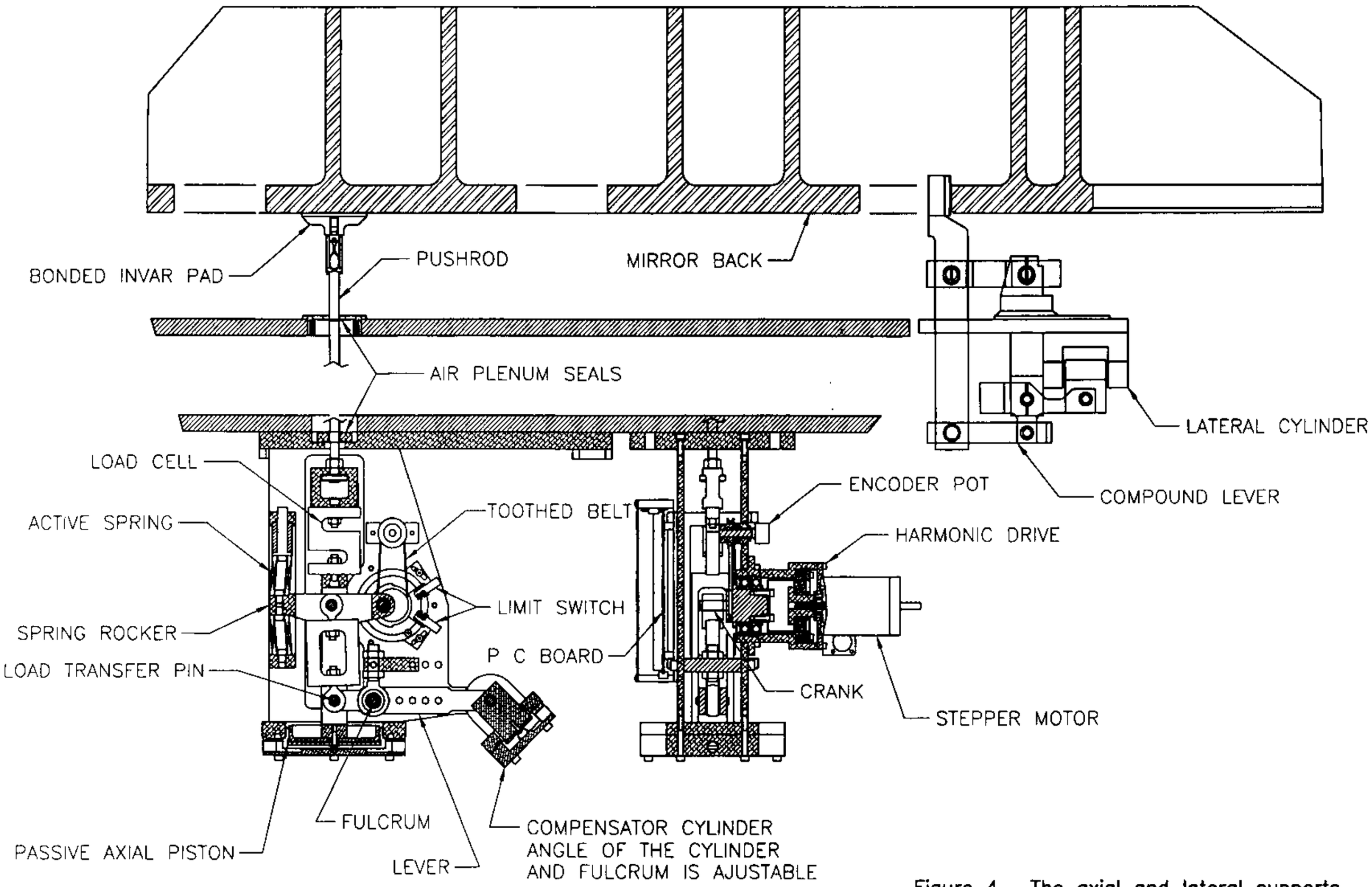

Figure 4. The axial and lateral supports.

The system uses 66 axial supports and 24 lateral supports to float the mirror against gravity (figures 3 & 4). Lateral supports apply forces at the back plate of the mirror and need work only in the elevation direction. Axial support units can apply push or pull forces to pucks bonded to the back plate of the mirror. Each axial support unit sums forces from three sources: a passive support piston, a smaller compensator piston which applies an adjustable force, and an actively controlled spring force. The sum of these forces is monitored by a load cell.

The compensator pistons are hydraulically connected to the lateral supports. As the telescope points away from zenith, some of the force developed by the mirror weight on the lateral support hydraulic pistons is transmitted to the axial supports through the compensator pistons. The sign and magnitude of this force is tuned by adjusting the mechanical leverage and by clocking the cylinder mounting angle. This compensates for hydrostatic head pressure and can also be used as a general correction for any elevation dependent effects.

The primary mirror support pistons are divided into three zones. Pistons within a zone are hydraulically interconnected to form a whiffle tree. Each zone connects to a reservoir through a metering pump or "make-up unit" to control the fluid level within the zone. The lateral supports are interconnected to a make-up unit to form a fourth zone. The distribution of forces within a whiffletree depends on the piston area, mechanical connection leverage, and hydrostatic head pressure on the piston. The summation of all forces in a zone is statically equal to the weight of the mirror upon the zone. The pistons can only generate force in one direction, so negative hydraulic pressure is not allowed.

3.2 Position, force, and pressure control loops

As the telescope changes elevation angle the mirror tends to move relative to its cell due to flexure of the cell and compliance in the support units. The position of the mirror relative to the cell is measured at four places using LVDT's. The control strategy is to maintain the LVDT readouts at at fixed values by using operating of the makeup units to adjust fluid levels in the four zones. In the control software this is called the position loop.

The most interesting part of the WIYN design is the force control loop which actively bends the mirror to control its figure. Axial forces applied to the mirror are measured by load cells placed between each support unit and the mirror. The load measured at each support is the sum of the passive and active forces. The active component is used as a "trim" or delta force added to optimize the shape of the mirror. The active mechanism can add or subtract a spring force by displacement of a lever driven by a rotating crank. The crank is turned by a stepper motor through a 160 to 1 Harmonic Drive transmission. The stiffness of the spring is low relative to the passive support, so that sensitivity to cell distortion is low. The force range is from 1110 newtons push to 876 newtons pull.

Active support forces must bend the mirror without changing the overall pressure in the zones, so the delta forces within a given zone must sum to zero. This is a boundary condition applied to the calculation of the active forces. This condition is also controlled by a pressure servo loop. Pressure in each axial zone is monitored by a transducer and compared to the theoretical value at a given elevation angle. Any difference is corrected by applying a pattern of delta forces to the zone in proportion to the passive axial piston areas. This corrects the zonal pressure without changing the mirror figure.

4. SECONDARY MIRROR AND SUPPORT

The 1.2 meter diameter secondary mirror is made of Zerodur lightweighted to about 28% of solid weight by machining hexagonal pockets into the back of the blank. The machining was done at the Schott Glasswerkes in Mainz, Germany. The resulting blank weighs 120 Kg. Lightweighting the mirror reduces thermal inertia and increases its rigidity, simplifying mirror support and handling.

Lateral support and definition of the mirror is provided by a central hub bonded to the glass. The hub is attached to the cell through a diaphragm flexure which is laterally stiff but axially compliant. Axial definition of the mirror is provided by three flexures bonded to the mirror at roughly the 70% radius. These flexures anchor the mirror to load cells mounted on the mirror cell. Output from the load cells is used to regulate the pressure of the air behind the mirror to provide axial support by floating the mirror on ambient air pressure. A rolling diaphragm with a zip-lock seal attaches the edge of the mirror to the lip of the mirror cell providing an air-tight seal. Choice of an inherently athermal support design allowed the use of aluminum for the structure of the mirror cell further reducing weight. The secondary mirror and cell together weigh 230 Kg.

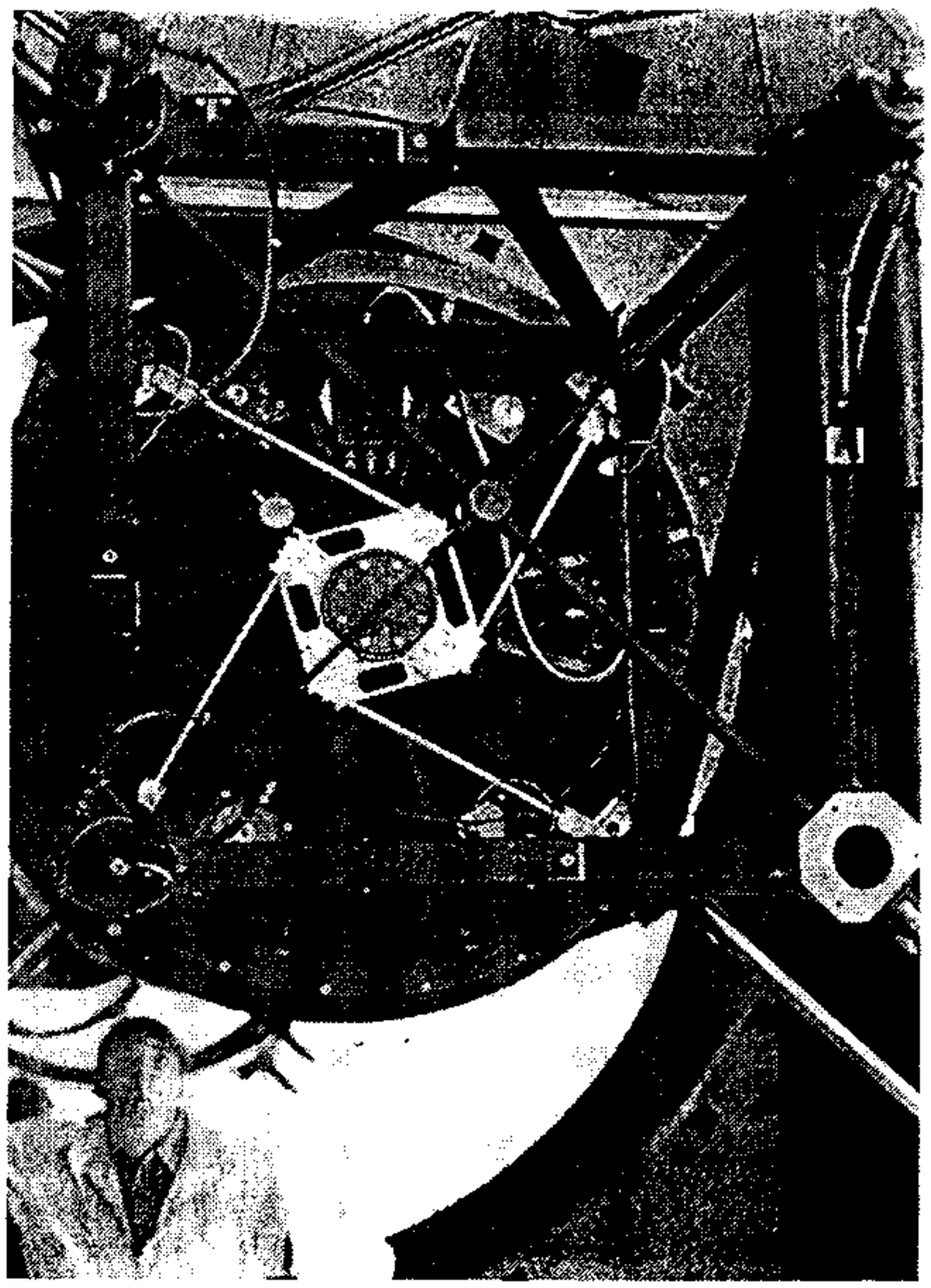

Figure 5. The secondary mirror cell.

4.1 Secondary mirror articulation

The secondary mirror cell is attached to the telescope structure in a manner analogous to the mounting of the mirror to its cell. The center hub of the secondary cell attaches to the corners of the secondary cage through four flexure bars arranged in a spiral "fireman's carriage" formation. This flexure is laterally stiff but axially compliant to allow up to 1.5 cm focus travel. It is also rotationally compliant to allow active tilt of the cell.

Three push/pull rods attach to the edge of the cell to provide axial definition and support of the cell. They are laterally compliant to allow for differential expansion between the aluminum cell and the steel cage. The push rods terminate at the top ends of the cage tubes in three linear actuators. Each actuator consists of a stepper motor, an 80:1 Harmonic Drive gear reducer, and a 2 mm pitch Transroll screw. This combination gives 0.125 microns of linear travel per whole step of the motor. All three actuators move together to piston the mirror for focus, or individually to tilt the mirror. When used individually one step results in about 0.014 arc-sec of angular field displacement. Shop tests showed that the hysteresis on reversal of motion is less than one micron (0.11 arc-sec).

Micro stepping is used for smooth acceleration and high speed operation, however the motors are stopped only at whole step increments. The magnetic detent torque of the motor is sufficient to prevent the actuators from back driving despite the high efficiency of the gear and roller screw. The motors are de-energized between traverses to reduce heat dissipation.

5. PRIMARY MIRROR CONTROL ELECTRONICS

High level control originates from a single processor located off the telescope while low level control electronics are distributed close to the system axes. Low-level tasks are constantly executed transparent to the high-level centralized functions. These include conditioning and reading load cells, generating waveforms for stepper motor control, and the like. An addressing scheme makes it is possible to command or query a single given actuator if desired.

A custom PCB was designed and built at NOAO to handle the tasks specific to the 8051 based controller. Heat dissipation is a critical factor since all the boards are mounted on the back of the mirror cell. CMOS technology was used throughout to limit power dissipation to about 2 Watts per board, lower by a large factor compared to similar commercial products. Figure 6 shows a block diagram of the PCB.

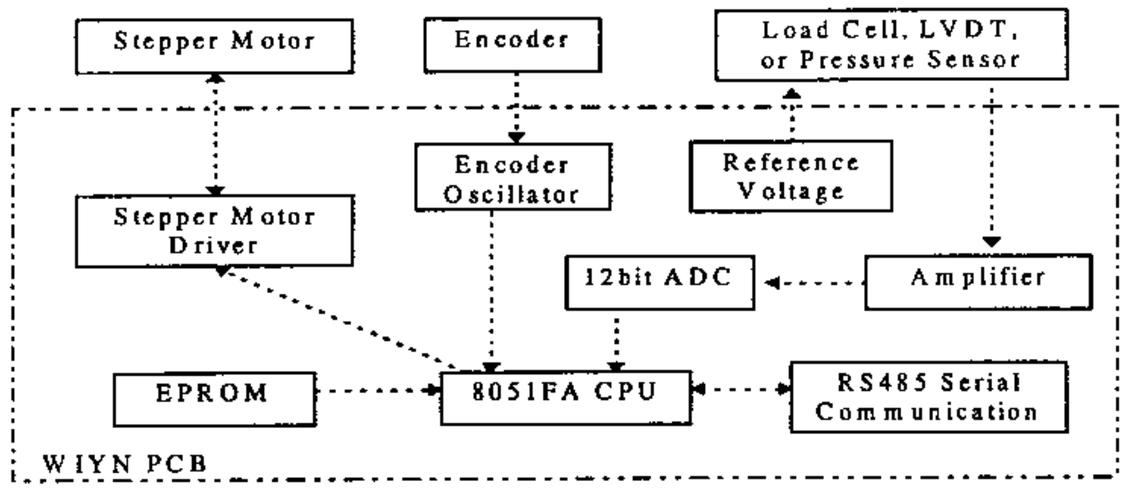

Figure 6. The WIYN electronics PCB block diagram.

Load cell, LVDT, and pressure readouts are performed through a single multi-use channel which provides reference and excitation voltages, a differential balanced preamplifier, and a 12 bit analog to digital converter. The force resolution is 0.6 Newtons (0.125 lb). The stepper motor driver is a chopping type in standard use at Kitt Peak, but repackaged using recent devices such as compact high current drivers and PAL's. Communication between the 74 units is via an RS-485 differential bus running at 38.4 KBd and a redundant protocol based on the SDLC scheme. For power distribution reasons, the units are grouped into 6 branches distributed into sectors on the mirror cell. A multiplex/demultiplex interface unit separates the multi-point low-level control from the single-point high-level control. The high-level control is performed in a Heurikon HKV3D computer running VxWorks (a real time unix-like operating system). System interface code was written to allow accessing an individual actuator. The high level functions include C calls for reading load cells, moving motors, performing diagnostics, and similar tasks. The VxWorks computer exchanges telemetry with other parts of the telescope control system via the WIYN message passing system. The complete active optics control hardware is depicted on figure 7.

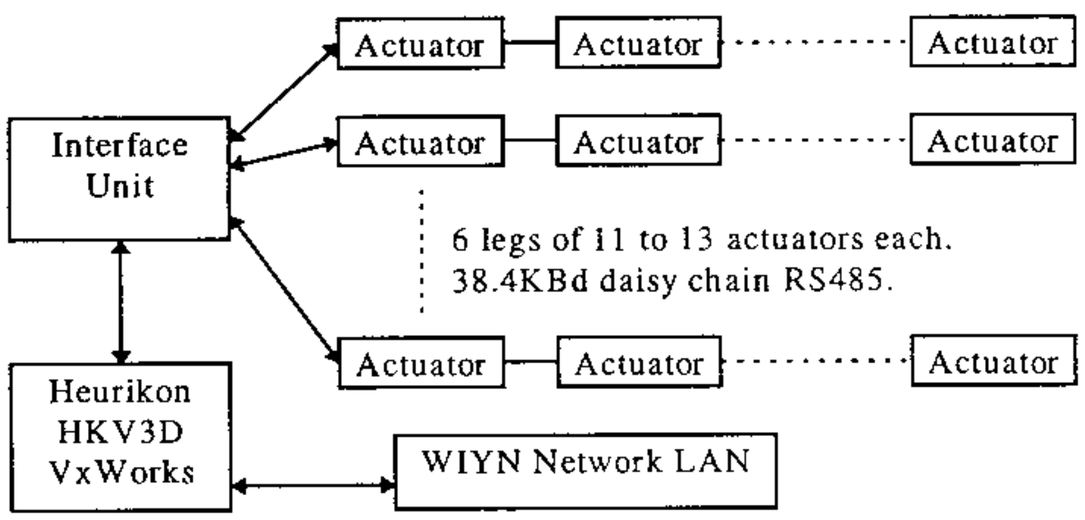

Figure 7. Active optics control hardware

6. WAVEFRONT SENSOR

The wavefront sensing technique used at WIYN is called "wavefront curvature sensing". It was first proposed by F. Roddier[10], and consists of comparing the illumination in two stellar images defocused in opposite directions. It can be shown that local differences in illumination are directly related to the local wave-front total curvature or Laplacian, whereas differences in the location of the aperture edge give a measure of the wave-front radial edge slope. The wave-front surface can be reconstructed by solving a Poisson equation using the estimated edge slopes as Newmann boundary conditions. The technique is often used to test astronomical telescopes. Most telescopes are now equipped with science-grade CCD cameras which can be used for that purpose. With an all reflecting telescope, no color filter is needed. Experience shows that an exposure time of at least 30 seconds to one minute is necessary to average out seeing effects.

A critical parameter is the distance from focus at which images are taken. This distance is chosen by trading sensitivity against spatial resolution. Currently the defocus is created by moving the secondary mirror 1500 microns on each side. This results in an equivalent 2 cm defocus in the focal plane. Later this approach will be replaced by placing a CCD camera on a motor-driven stage that can traverse through focus.

The larger the amount of defocus the higher the spatial resolution on the reconstructed wave front, but the lower the sensitivity to aberrations. A defocused stellar image can be viewed as a blurred pupil image. To a good approximation the amount of blur is given by the size of the in-focus image. The ratio of the diameter of the defocused image over the diameter of the best focused image is therefore a measure of the maximum number of resolved wave-front elements across a pupil diameter. For this application we need at least 66 resolution elements over the whole pupil area, i.e. about 10 resolution elements across the diameter. To avoid aliasing errors, the sampling interval should be at least two times smaller. This gives a minimum of 20 pixels across a diameter. In practice, we use about 40 pixels.

The data processing algorithm has already been described in the literature[11]. It is summarized here in a flow chart shown on figure 8. The two images are recentered, subtracted, and a first wave-front estimate is obtained by solving a Poisson equation. This is done by means of fast Fourier transforms[12]. A tilt error and a defocus error are determined, and used to recenter and rescale the defocused images. Then a geometrical transformation is applied to compensate the estimated effect of the aberrations. The two images are again subtracted and a new wave-front estimate is computed. The same operations are iterated until the new wave-front differs from the previous one by less than a given amount (typically 0.01 micron). In practice, the final wave front surface is obtained in 5 or 6 iterations.

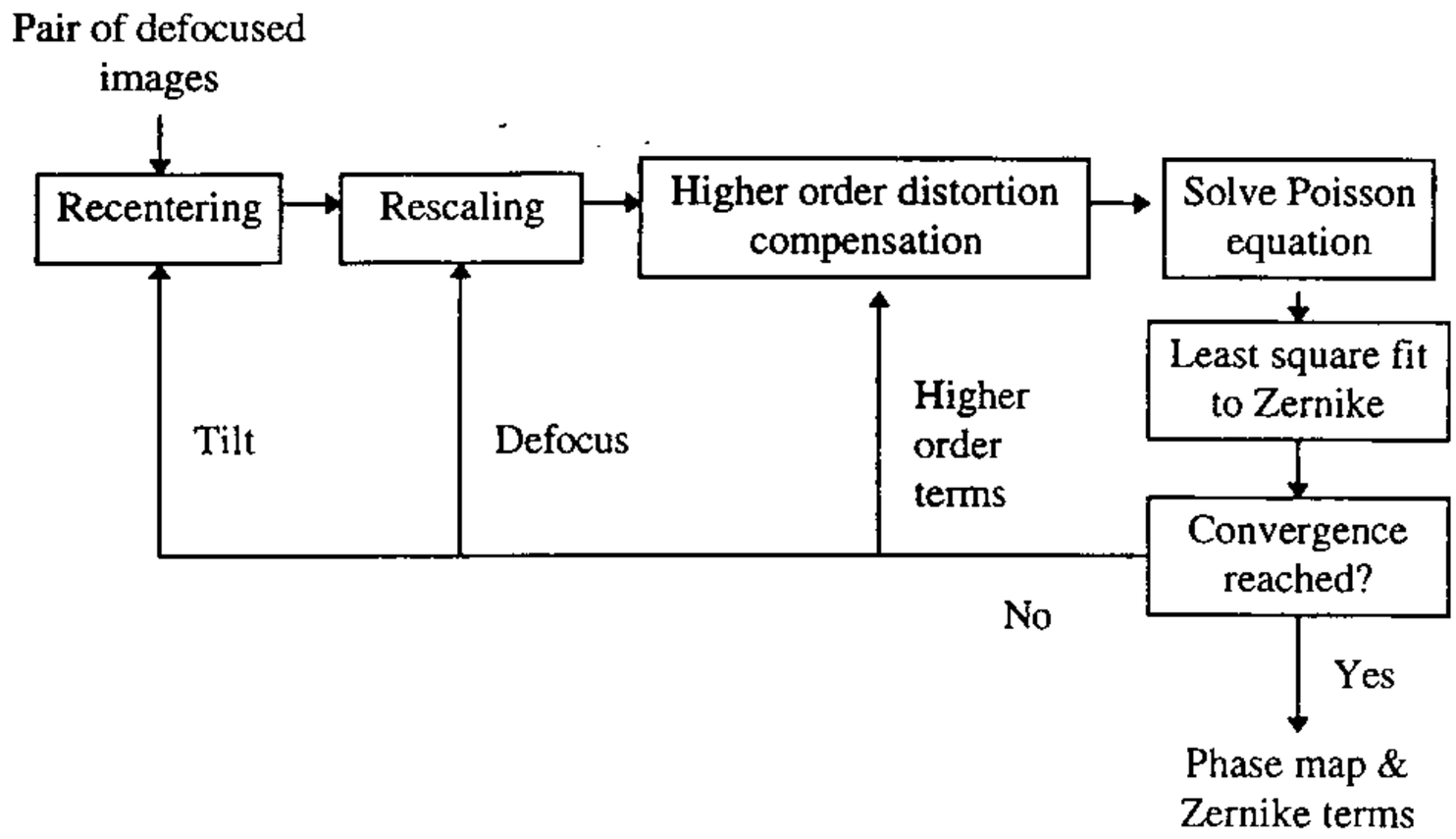

Figure 8. Flowchart for the wavefront algorithm.

7. CONTROL ALGORITHMS

In this section, we describe the algorithms used to control the active optics. First we describe the algorithms specific to the control of the primary mirror figure. In the next section we describe the control of the active collimation of the telescope.

7.1 Primary figure control

Initial tests of the system relied on modes that were developed from finite element analysis (FEA) of a model of the primary mirror. Discrepancies between the model and the real system were observed and the control forces were large in magnitude, typically 440 Newtons. We decided to change strategy. An empirically derived mode set was needed.

Assuming a linear system, an interaction matrix M is defined as the matrix that relates an observed output o to an influence input i: $o=M*i$. The matrix M can be built by successively producing test force patterns and measuring resulting output. Once the interaction matrix is built, modal analysis can be used to determine the best set inputs (influences) to achieve a given output. In this case we define the "best" set as applying the lowest force to the mirror.

Several types of matrices have been built and have particular characteristics. It is obvious from a mechanical point of view that the higher the order of correction, the higher the magnitude of forces to be applied. A first matrix of order 12 was constructed. Every one of the 66 actuators was excited in turn, and its response recorded on a grid of 292 points. The resulting 292 x 66 matrix had its order reduced to 12 through a singular value decomposition (SVD). Among the 12 modes that were retained were natural astigmatism and natural trefoil, the other ones not having an obvious relation to usual optical modes. Coma was intentionally left out since, as it will be shown in the next section, it is controlled with the secondary mirror.

Corrections based on the empirically derived interaction matrix were as effective as with the initial matrix derived from the FEA, but typical forces were reduced to about 140 Newtons. This was mostly due to limiting the order of the modes. Higher order modes require higher forces for very little correction. This led us to construct a second matrix of even lower order - order two. This low order matrix can only correct astigmatism. The reasoning for this matrix is that once the system is tuned to remove aberrations up to order 12, disturbances produce mostly astigmatism. Correcting only the astigmatism allows us to maintain good correction with very small changes in the force matrix.

This matrix was built by binning the actuators into 9 groups. Each group was excited in turn and the corresponding 292 x 9 matrix assembled. Again using an SVD, the order of the matrix was reduced to 2. Using this interaction matrix the correction forces are further reduced to the 25 Newton range. However, modes such as trefoil can't be corrected using this matrix. Our experience from on-site operation has shown that random disturbances generally do not cause trefoil, however astigmatism and coma are common.

Calibration of the primary therefore involves the construction of two matrices: a 12th order matrix to be used when high order aberrations are present, and a second order matrix to be used when the system is behaving well. In practice, the latter is in regular use.

To date we have done two calibrations of the interaction matrices. The second calibration was done after extensive rework of the primary mirror support units to eliminate leaks. Indications are that the interaction matrix is stable for several months at a time, but may need to be remeasured periodically.

7.2 Collimation

Miscollimation of the secondary from the primary optical axis generally results in coma evenly distributed over the field. The WIYN image error budget allocated 0.1 rms image enlargement worst case anywhere over a one degree diameter field for effects due to miscollimation. Ray traces indicated that decenters as large as 0.21 mm could be compensated by adjusting only the tilt of the secondary mirror without exceeding the image error budget. Tilting the secondary to remove coma can leave residual aberrations dominated by tilt of the wavefront defocusing the images at the edges of the one degree field. Active collimation using only tilt of the secondary mirror greatly simplifies the mechanics and control electronics.

Anticipating active control of the secondary tilt led to two strategies in the design of the telescope structure: the forward tube truss and secondary spider were designed to be rigid, and flexures were built into the attachment points of the primary mirror cell to passively control the tilt of the mirror cell. Each of the four mirror cell attachment posts incorporate a diaphragm flexure. These flexures were "tuned" during the finite element design phase to keep the primary axis pointing towards the secondary vertex as the telescope rotates through the gravity field. This differs from a classical Serrurier truss in which the sag of the primary mirror cell support is matched to the sag of the forward truss. Tilt control can be done with displacements which are much smaller than the overall sag of the truss, so the WIYN design results in a structure with higher resonant frequencies than a classic Serrurier design.

The design of the secondary mirror focus/tilt stage places the pivot point about 400 mm above the secondary vertex. Tilting the secondary to correct for coma results in angular field displacement which in turn is corrected by repointing the telescope. For a decentration d of the secondary away from the primary axis, the amount of secondary tilt B needed to remove coma is given by

$$B = d / (VC-VP) \tag{1}$$

where VP is the distance from the secondary vertex to the pivot point and VC the distance from the secondary vertex to the "zero coma point". For Ritchey-Chretien and Cassegrain telescopes the zero coma point is very nearly coincident with the telescope prime focus.

The angular field displacement A due to a secondary tilt about an arbitrary pivot point is given by

$$A = -B(R2 - VP)(M-1)/F \tag{2}$$

where R2 is the secondary radius of curvature, M the system magnification, and F the system focal length.

As implemented, secondary tilt and focus corrections are calculated by the primary mirror processor based on a look up table or on a wavefront reduction. The primary processor issues commands to a secondary mirror processor that calculates the proper pointing offset associated with the commanded tilt. The secondary processor then issues a pointing offset command to the telescope control system, and a command to the low level controller which tilts the secondary mirror. These processes run asynchronously, so the pointing offset and secondary tilt are not smoothly coordinated. However, since the look up tables are interpolated every seven seconds, the offset commands are very small, typically of order 0.01 arc-sec, and there is no noticeable degradation in telescope tracking.

8. OPERATIONS

During engineering trials the operation of the active optics has evolved along lines somewhat different from what was envisioned at the start of the project. In general the system is tending towards greater simplicity.

In practice we begin each night with a wavefront measurement. This is decomposed into Zernike polynomials and the coma and focus terms extracted for processing by the secondary mirror controller. After correcting the coma and focus, a second wavefront measurement is done. We judge whether the remaining aberrations are large enough to warrant correction with the primary mirror. If only astigmatism is present, a second order matrix is used to compute a corrective force set. If higher order aberrations are present the 12th order matrix is used. Terms of order greater than 12 are very small due to the excellent intrinsic quality of the polished optics and are ignored.

8.1 Open vs closed loop operation

We anticipated that the active optics system would operate with a combination of open loop corrections from look up tables and frequent real time adjustments to keep the system tuned. In practice we have found that few real time adjustments are needed. After tuning at the start of the night the system tends to stay tuned for hours at a time.

On opening we typically find up to a wave of coma that is corrected by tilting the secondary. Often this is the only correction needed to yield a wavefront of 200 nm rms or better. Occasionally we find astigmatism; less frequently we find higher order aberrations such as trefoil that require correction using the 12th order matrix. Trefoil usually results from systematic problems in the support of the secondary, tertiary or primary mirrors. The sudden appearance of trefoil in the wavefront has led us to search for mechanical causes rather than making immediate corrections to the primary figure.

We have found that a look up table will provide good correction for several months, however there is a gradual degradation in the accuracy of the corrections due in part to thermal effects and seasonal changes of load cell calibrations. New lookup tables must be built periodically.

8.2 Building lookup tables

For convenience the zero point for the table is set at 80° elevation. We start the process by taking wavefront measurements to correct both the secondary collimation and primary figure. Several iterations are often done to achieve the best possible wavefront. When it is "good enough" the applied primary forces and secondary positions are recorded. The telescope is then moved to an elevation of 60° and the optics are re-optimized. After completion the telescope is moved back to 80° and optimized again. The whole procedure consists of optimizing the system at 80, 60, 80, 40, 80, 20, 80° elevation. Lookup table entries are calculated as the difference from the zero point to a given angle. This tends to eliminate systematic effects on the measurements such as temperature gradients. Despite this precaution, we have found that lookup tables need to be built late in the night when thermal variations have reached equilibrium.

The lookup table contains secondary position and primary mirror delta force vectors for optimal performance at 80, 60, 40 and 20° elevations. Interpolation is used for intermediate elevation angles. Extrapolation extends the table to 89.6° and down to 15° covering the full range of the telescope.

9. RESULTS

Figure 9 shows two plots of the wavefront measurements taken over January 1995. The first plot records the measured rms wavefront error, the second plots the Zernike aberrations in waves. The date and sample number form the abscissa. Typically on opening we find fairly large aberrations which are reduced in one or two iterations. In the first iteration the secondary mirror is repositioned to remove coma and focus. Often this is enough to achieve a wavefront better than 200 nm rms. If needed, a second iteration is done to optimize the primary mirror figure. The median value of the 29 wavefront measurements

taken over January was 181 nm rms. The large (1 wave) trefoil on the night of Jan 28 was due to an error in the secondary support, the pressure regulator was inadvertently turned off.

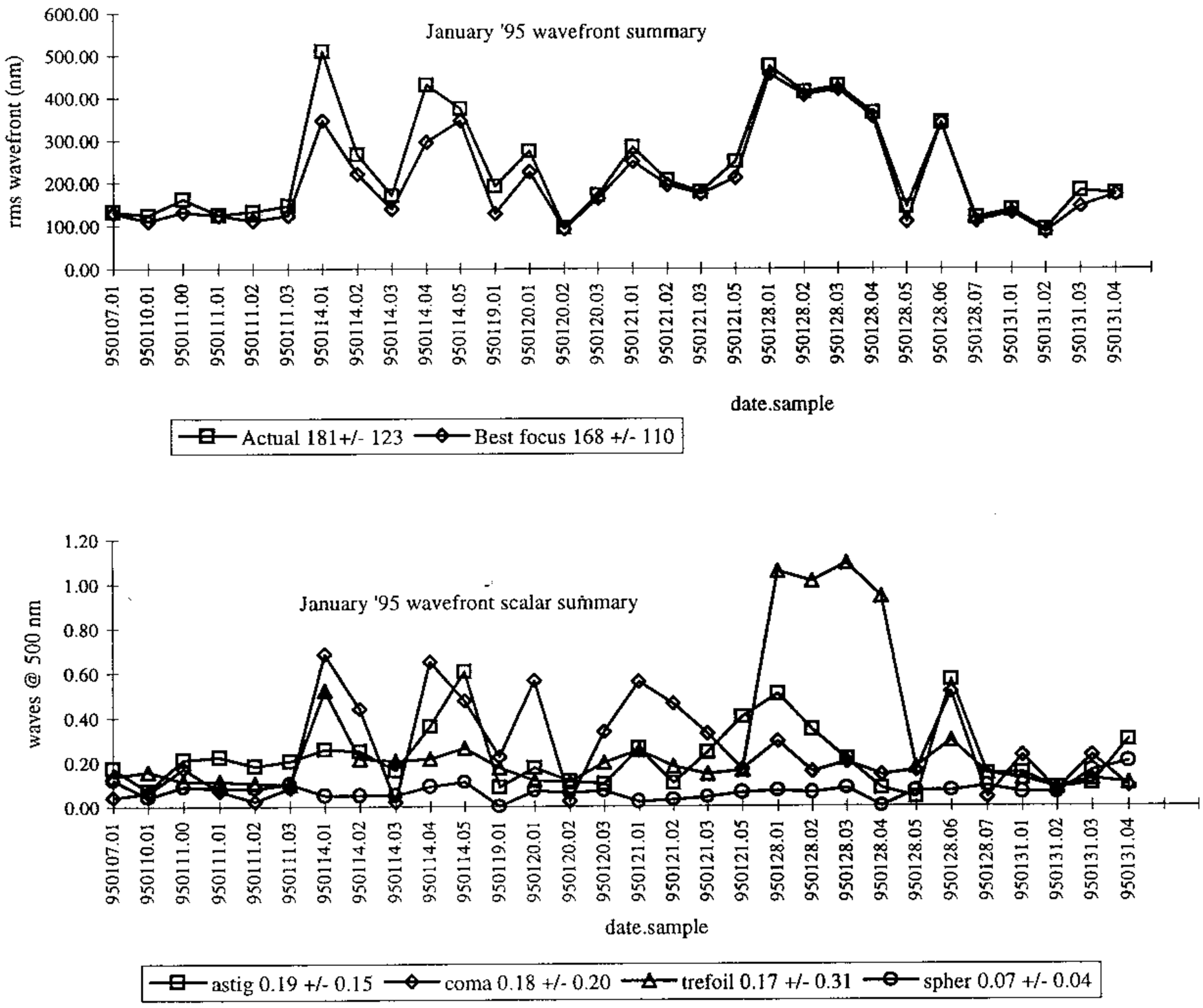

Figure 9. Rms wavefront values and individual aberrations measured at WIYN.

The active optics system maintains the quality of the optical train so that delivered image quality (DIQ) is typically limited by seeing rather than by the optics. We are still compiling statistics on wavefront quality and DIQ. Our impression is that the threshold of seeing-limited performance is about 200 nm rms wavefront most of the time. With the telescope optics tuned to deliver wavefronts better than this threshold, there is little correlation between the measured wavefront and the actual DIQ. For example, we have been able to obtain wavefronts better than 100 nm rms on nights when the DIQ was no better than 1 arc-sec. On the other hand, when the active optics have been tuned to levels around 150 nm rms we have occasionally obtained images better than 0.5 arc-sec FWHM.

In-focus images have been routinely obtained with a CCD imaging camera and measured with the IMEXAMINE tool in IRAF, the image reduction analysis facility written and maintained at NOAO. IMEXAMINE fits a Gaussian through an intensity profile of the image, using the curve fit to determine full width at half maximum. Statistics based on 72 images taken from June, 1994 to January, 1995 are summarized in figure 10, which shows a histogram of the DIQ. The median DIQ for the site measured to date is 0.7 arc-sec FWHM. Sample astronomical images obtained at WIYN are shown on figure 11.

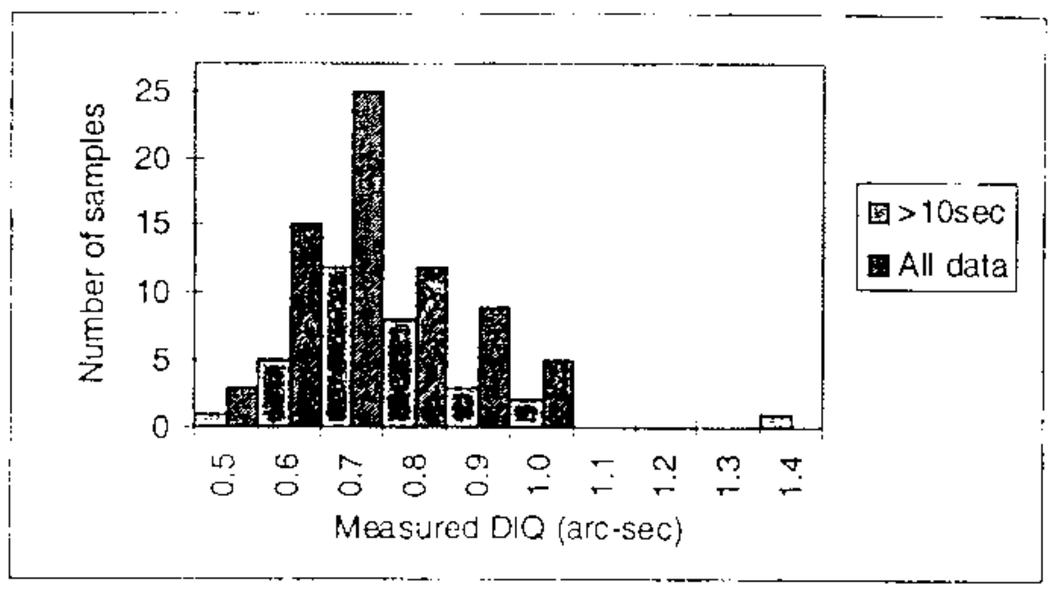

Figure 10. Statistics of measured delivered image quality (DIQ) at WIYN.

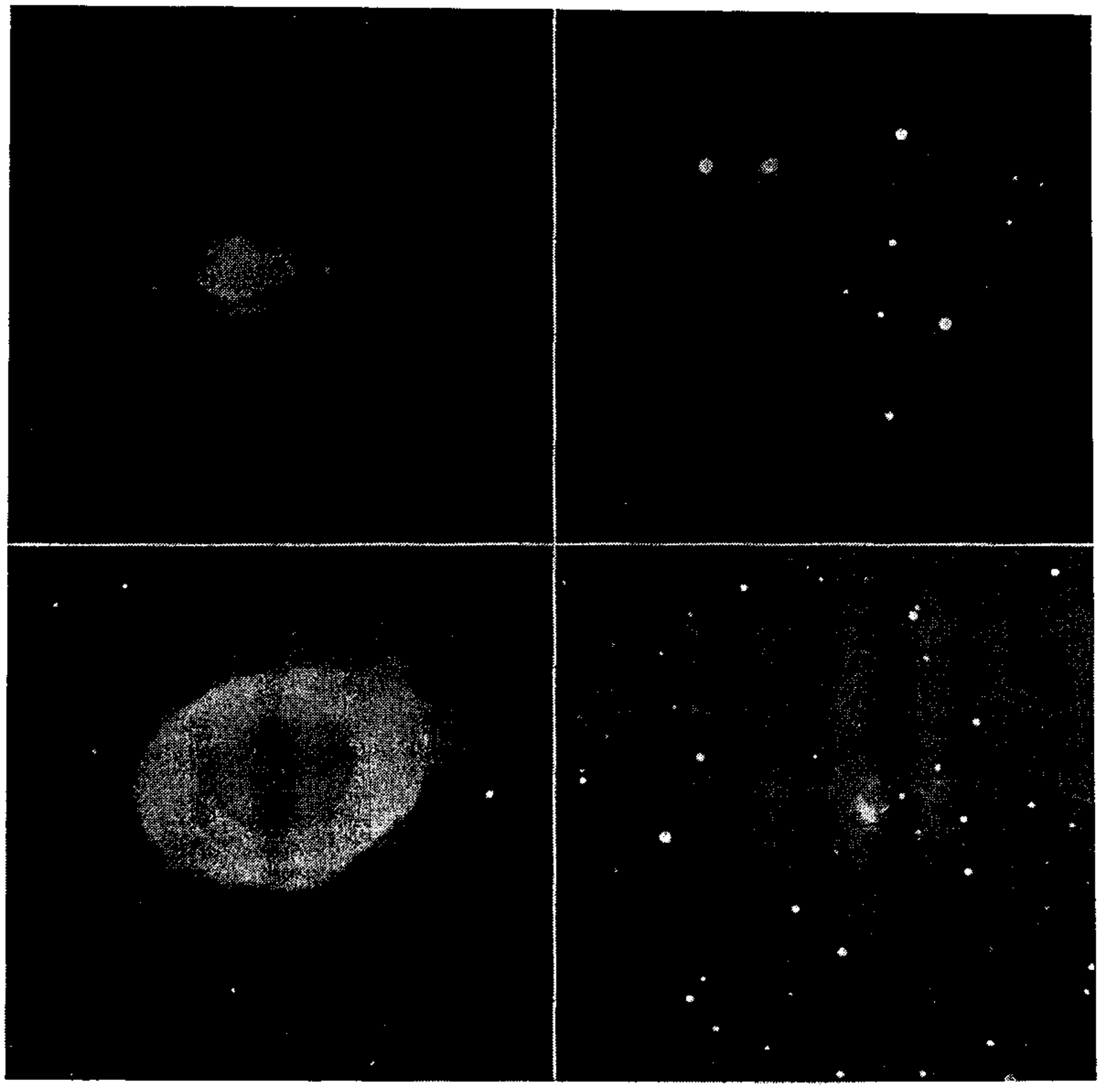

Figure 11. Sample astronomical images obtained at WIYN.
Saturn Nebula (NGC 7009), Arp 273,
Ring Nebula (NGC 6720), Spiral Galaxy NGC 2276

10. SUMMARY

We have described the components, control algorithms and operational experience with the WIYN active optics system. Though we are not yet in science operations, results obtained to date have shown that the system is operating very well. The quality of images obtained have exceeded many of our expectations for the performance of the telescope and of the site.

The WIYN active optics has proven to be an important part of an integrated over-all design that includes attention to the thermal design of the facility and particular care in the fabrication of optics.

11. ACKNOWLEDGMENTS

A full list of all the people who contributed to the WIYN telescope would be too long to publish here. However, we would to acknowledge the particular contributions of Dave Dryden, Alex McDonald, Dave Sawyer, Dave Silva, Bridget Watts, and Richard Wolff.

12.REFERENCES

1. M. Johns and C. Pilachowski, "The WIN 3.5 Meter Telescope Project", Advanced Technology Optical Telescopes IV, vol. 1236, SPIE, Tucson, 1990.

2. M. Johns and D. Blanco, "The WIYN 3.5 Meter Telescope Project", Advanced Technology Optical Telescopes V, vol. 2199, SPIE, Kona, 1994.

3. D. Anderson, J. Burge, D. Ketelsen, B. Martin, S. West, G. Poczulp, J. Richardson, W. Wong, "Fabrication and testing of the 3.5m, f/1.75 WIYN primary mirror", Advanced Optical Manufacturing and testing IV, vol 1994, SPIE, San Diego, 1993.

4. L. Goble, "Temperature Control of the 3.5-Meter WIYN Telescope Primary Mirror", Analysis of Optical Structures, vol. 1532, SPIE, San Diego, 1991.

5. D. Blanco and M. Johns, "Thermal Design of the WIYN 3.5 Meter Telescope Enclosure", Advanced Technology Optical Telescopes V, vol. 2199, SPIE, Kona, 1994.

6. L. Stepp, "3.5m Mirror Project at NOAO", Advanced Technology Optical Telescopes IV, vol. 1236, SPIE, Tucson, 1990.

7. L. Stepp, N. Roddier, D. Dryden, and M. Cho, "Active Optics System for a 3.5-meter Structured Mirror", Active and Adaptive Optical Systems, vol. 1542, SPIE, San Diego, 1991.

8. L. Goble, G. Poczulp, N. Roddier, and L. Stepp, "Results of testing the 3.5m WIYN Telescope Primary Mirror and its Support, Thermal Control, and Active Optics Systems", Proceedings of the ESO workshop on Progress in Telescope and Instrumentation Technologies, Garching, 1992.

9. L. Goble, R. Angel, J. Hill, E. Mannery, "Spincasting of a 3.5m diameter f/1.75 mirror blank in borosilicate glass", Advances in Fabrication and Metrology for Optics and Large Optics, vol. 966, SPIE, pp 300-308.

10. F. Roddier (1988), "Curvature sensing and compensation: a new concept in adaptive optics", Appl. Opt. , Vol. 27 (No 7), pp. 1223-1225.

11. F. Roddier, C. Roddier (1991), "Wave-front reconstruction using iterative Fourier transforms", Appl. Opt. , Vol. 30 (No 11), pp. 1325-1327.

12. C. Roddier, F. Roddier (1993), "Wave-front reconstruction from defocused images and the testing of ground-based telescopes", J. Opt. Soc. Am. A , Vol. 10 (No 11), pp. 2277-2287.